A vital role of tubulin-tyrosine-ligase for neuronal organization

Christian Erck*†, Leticia Peris†‡, Annie Andrieux†‡, Claire Meissirel§, Achim D. Gruber¶‖, Muriel Vernet**, Annie Schweitzer‡, Yasmina Saoudi‡, Hervé Pointu**, Christophe Bosc‡, Paul A. Salin††, Didier Job‡,‡‡, and Juergen Wehland*‡‡§§

*Department of Cell Biology, German Research Center for Biotechnology, D-38124 Braunschweig, Germany; ‡Laboratoire du Cytosquelette, Institut National de la Santé et de la Recherche Médicale U366, and **Atelier de Transgenèse, Département Réponse et Dynamique Cellulaire, Commissariat à l'Energie Atomique, F-38054 Grenoble, France; §Institut National de la Santé et de la Recherche Médicale U433 and ††Unité Mixte de Recherche 5167, Centre National de la Recherche Scientifique, Faculté de Medecine, RTH Laennec, F-69372 Lyon, France; and ¶Department of Pathology, School of Veterinary Medicine Hannover, D-30559 Hannover, Germany

Edited by Ronald D. Vale, University of California, San Francisco, CA, and approved April 21, 2005 (received for review December 22, 2004)

Tubulin is subject to a special cycle of detyrosination/tyrosination in which the C-terminal tyrosine of α-tubulin is cyclically removed by a carboxypeptidase and readded by a tubulin-tyrosine-ligase (TTL). This tyrosination cycle is conserved in evolution, yet its physiological importance is unknown. Here, we find that TTL suppression in mice causes perinatal death. A minor pool of tyrosinated (Tyr-)tubulin persists in TTL null tissues, being present mainly in dividing TTL null cells where it originates from tubulin synthesis, but it is lacking in postmitotic TTL null cells such as neurons, which is apparently deleterious because early death in TTL null mice is, at least in part, accounted for by a disorganization of neuronal networks, including a disruption of the cortico-thalamic loop. Correlatively, cultured TTL null neurons display morphogenetic anomalies including an accelerated and erratic time course of neurite outgrowth and a premature axonal differentiation. These anomalies may involve a mislocalization of CLIP170, which we find lacking in neurite extensions and growth cones of TTL null neurons. Our results demonstrate a vital role of TTL for neuronal organization and suggest a requirement of Tyr-tubulin for proper control of neurite extensions.

CLIP170 | tubulin code

Microtubules are essential components of the cell cytoskeleton and are centrally involved in cell division, cell motility, cell morphogenesis, and intracellular motile events. The α/β-tubulin dimer, the microtubule building block, is subject to specific posttranslational modifications that principally affect the C termini of both subunits (1). One of these modifications, the tyrosination cycle, involves the enzymatic cyclic removal of the C-terminal tyrosine of α-tubulin by a so far uncharacterized tubulin carboxypeptidase and the readdition of a tyrosine residue by the tubulin-tyrosine-ligase (TTL) (2, 3). This tyrosination cycle is conserved among eukaryotes (4, 5) and generates two tubulin pools: intact tyrosinated α-tubulin (Tyr-tubulin) and detyrosinated α-tubulin (Glu-tubulin), which lacks the C-terminal tyrosine. In cultured cells, Glu-tubulin is enriched in stable microtubules exhibiting little dynamic behavior (6–8), whereas dynamic microtubules display Tyr-tubulin. In cells with very long-lived microtubules, Glu-tubulin is finally converted into Δ2-tubulin, which lacks a C-terminal Glu-Tyr dipeptide and cannot be enzymatically converted back to either Glu- or Tyr-tubulin (9, 10). Under physiological conditions, Δ2-tublin is principally found in neurons but can also appear in cells lacking TTL activity, irrespective of microtubule stabilization (10). Tubulin detyrosination is a consequence, not the cause of microtubule stabilization (11). TTL is frequently suppressed during tumor progression (12–14) with resulting accumulation of Glu-tubulin in tumor cells. TTL suppression in human cancers is associated with increased tumor aggressiveness (13, 14). However, it is still unknown whether the tyrosination cycle is of any physiological significance in normal cells, tissues, or organisms. To test the importance of the tyrosination cycle in whole animals directly, we generated TTL null mice. These mice die shortly after birth, apparently because of disorganization of neuronal networks, indicating a vital role of TTL for the control of neuronal organization.

Materials and Methods

TTL Targeting Construct and Knockout Mice. Genomic DNA clones were identified as described (15). Within the targeting vector pPNT (16), in a 14-kb genomic clone (Fig. 1*A*) exon 1 was replaced by a phosphoglycerate kinase-driven neomycin resistance (*pGK-neo*) cassette. After electroporation into R1 ES cells (17) recombinant ES clones were identified by BamH1 digestion and hybridization with a BamH1–BglII probe (Fig. 1*A*). Two recombinant ES clones were aggregated with OF1 morula to generate chimeric mice (17). Germ-line-transmitting mice from the two ES clones were mated with either BALBc or 129 SvPas mice to produce heterozygous mutant mice on either mixed BALBc/129 SvPas or pure 129 SvPas backgrounds.

Antibodies, Western Blots, and TTL Assay. Primary antibodies used were Glu- and Δ2-tubulin (10), N STOP 175 (18), Tyr-tubulin (cloneYL1/2, provided by J. V. Kilmartin, Medical Research Center Laboratory of Molecular Biology, Cambridge, U.K.), CLIP170 [clone 4D3 (19)], EB1 (Transduction Laboratories, Lexington, KY), GFP (Molecular Probes), tau (Upstate Biotechnology, Lake Placid, NY), and TTL [clone 1D3 (20)]. For Western blot analysis amounts of tubulin protein in tissue lysates were estimated by using the non-C-terminal-recognizing monoclonal α-tubulin antibody (clone α3a) from the laboratories of D.J. and J.W. TTL activity in tissue extracts was determined as described (20). Immunoblots were analyzed by luminometry with a cooled charge-coupled device camera (Fuji) by using AIDA software (Raytest, Straubenhault, Germany).

Histology. Whole brains from embryos were fixed in 4% paraformaldehyde and embedded in paraffin. Coronal serial paraffin sections (5 μm) were stained with hematoxylin and eosin.

This paper was submitted directly (Track II) to the PNAS office.

Freely available online through the PNAS open access option.

Abbreviations: TTL, tubulin-tyrosine-ligase; dil, 1,1′-dioctadecyl 3,3,3′3′-tetramethylindocarbocyanine perchlorate; E*n*, embryonic day *n*; siRNA, small interfering RNA; IC, internal capsule; DTB, diencephalic-telencephalic boundary.

†C.E., L.P., and A.A. contributed equally to this work.

‖Present address: Department of Veterinary Pathology, Free University Berlin, D-14163 Berlin, Germany.

‡‡The laboratories of D.J. and J.W. contributed equally to this work.

§§To whom correspondence should be addressed. E-mail: wehland@gbf.de.

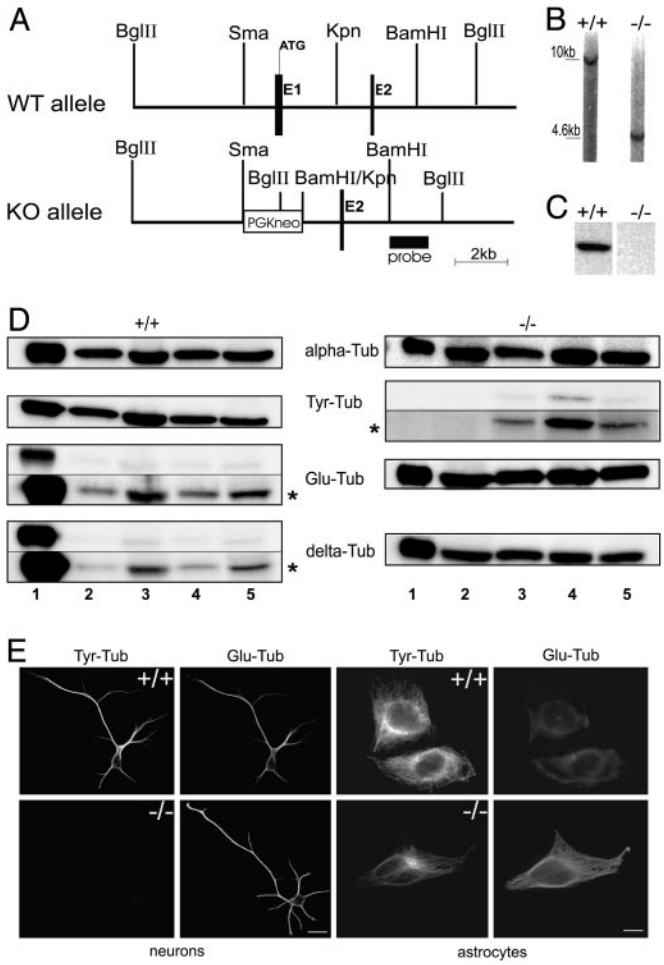

Fig. 1. TTL null mice. (*A*) Schematic representation of the *TTL* targeting vector and its genomic integration. (*B*) Southern blot analysis of genomic DNA derived from tails of newborn WT (+/+) and TTL null (−/−) mice after digestion with BglII and hybridization with the probe shown in *A*. (*C*) Western blot analysis of TTL in brain tissue of E19 WT and TTL null mice. Equal amounts of total protein were loaded. (*D*) Representative Western blot analysis of Tyr-, Glu- and Δ2-tublin in tissue lysates of E19 WT and TTL null mice ($n = 3$ for each phenotype). Tubulin loading was checked by using the α-tubulin mAb α3a (alpha-Tub). Lane 1, brain; lane 2, heart; lane 3, lung; lane 4, muscle; and lane 5, skin. Δ2-Tublin (delta-Tub) is present in all investigated TTL null tissues; minor amounts of Tyr-tubulin (Tyr-Tub) were detectable in TTL null tissues, especially in muscle, and Δ2-tublin was detected in WT tissues upon prolonged blot exposure. Blot exposure time was 10 s, except 60 s at *. (*E*) Analysis of tubulin composition in WT or TTL null brain cells. Double-immunostaining of Tyr- and Glu-tubulin in WT and TTL null hippocampal neurons or astrocytes in culture. Whereas only Glu-tubulin is detectable in TTL null postmitotic neurons, dividing astrocytes reveal Glu- and Tyr-tubulin (see Fig. 7 for higher magnification). (Scale bar: 20 μm.)

1,1′-Dioctadecyl 3,3,3′3′-Tetramethylindocarbocyanine Perchlorate (DiI) Labeling. The fluorescent carbocyanine dye diI (Molecular Probes) was used to trace projections in fixed WT and TTL null brains (21) at embryonic day 15 (E15) and E17 ($n = 2$ for each phenotype and each developmental stage). Brains were fixed in 4% paraformaldehyde and hemisected along the sagittal midline. Both hemispheres were used for axonal tracing. Crystals (50- to 100-μm diameters) were placed in the thalamus or the dorsal cortical plate of paired littermates. Brains were kept at 37°C for 5–8 weeks to allow appropriate diI diffusion. DiI-labeled axons were visualized under epifluorescence microscopy; for terminal axonal arbors a confocal microscope was used.

Cell Culture and Immunofluorescence Microscopy. Cortical and hippocampal cell cultures were prepared as described (22). Cells were plated on poly-L-lysine-coated coverslips in DMEM/10% FBS, which was replaced 2 h later by DMEM with B27/N2 supplement (GIBCO). Primary glial cultures were established from newborn mouse cerebral hemispheres (23). Cells were maintained in DMEM/10% FBS for 7 days to form an astroglial cell layer, with progenitor glial spread on top. Astrocyte cultures were derived from the astroglial cell layer. Mouse embryonic fibroblasts were prepared from E13.5 embryos following standard procedures and cultured in DMEM/10% FBS. For immunofluorescence, cells were either fixed with methanol (−20°C) or 4% paraformaldehyde and permeabilized with 0.1% Triton X-100. F-actin was visualized with rhodamine-phalloidin (Molecular Probes). Fluorescence intensity ratios were determined by using METAMORPH software, version 6.2 (Universal Imaging, Downingtown, PA).

Small Interfering RNA (siRNA). siRNA oligonucleotides specific for the six mRNAs encoding α-tubulin with a C-terminal Tyr were designed as described (24): tuba1 (GenBank accession no. NM_011653), tuba2 (GenBank accession no. NM_011654), tuba3 (GenBank accession no. NM_009446), tuba6 (GenBank accession no. NM_009448), tuba7 (GenBank accession no. NM_009449), and tuba8 (GenBank accession no. NM_017379). We used the combination of two siRNAs specific for α-tubulin tuba1, tuba2, and tuba6 (siRNA A and B) and of two siRNAs specific for α-tubulin tuba3, tuba7, and tuba8 (siRNA C and D). siRNA sequences are: siRNA A, AACGAAGCCATCTACGACATC (coding region 616–636); siRNA B, AAATACATGGCCTGCTGCATG (coding region 931–951); siRNA C AAAGAAGTCCAAGCTGGAGTT (coding region 486–506); and siRNA D AAAGATGTCAATGCTGCCATT (coding region 976–996).

siRNA oligonucleotides were purchased from Proligo (Paris). Transient transfection of siRNA (200 nM) was carried out in serum-free media by using Oligofectamine (Invitrogen). Ten percent FBS was added 3 h after transfection, and cells were cultured for 48 h.

Time-Lapse Video Microscopy and Morphometric Analysis. Hippocampal cells from WT or TTL null embryos were cultured for up to 5 days and maintained with serum-free DMEM plus 20 mM Hepes and supplement B27/N2 inside the video microscopy platform. Phase-contrast images were taken every 15 min for 3 days. Neurite and axon lengths were measured by using METAMORPH. Neuritic growth rates were determined as the slope of the regression of neuritic length vs. time. Neuritic length variations were measured as the linked variance of neuritic length around the linear regression of length vs. time. A similar procedure was applied for axonal length variations. To measure neurite length, antibody- or phalloidin-labeled cells were randomly selected from fixed cells on coverslips and analyzed by METAMORPH. The following parameters were evaluated: axonal length, length of minor processes, and percentage of neurons having two axons. We examined >100 cells from three independent cultures for each experimental condition and time point.

Results

TTL Null Mice. TTL null mice were generated by conventional gene knockout by insertion of a neomycin selection cassette into the first exon of the ubiquitously expressed *TTL* gene (Fig. 1 *A* and *B*). Heterozygotic mice were normal, and crossing of heterozygotes yielded all expected genotypes in a Mendelian ratio at birth, indicating that deletion of TTL was not embryonically lethal. Newborn TTL null mice, either from 129 SvPas/BALB/c or 129 SvPas pure backgrounds, were indistinguishable from their WT littermates with apparently normal organogenesis.

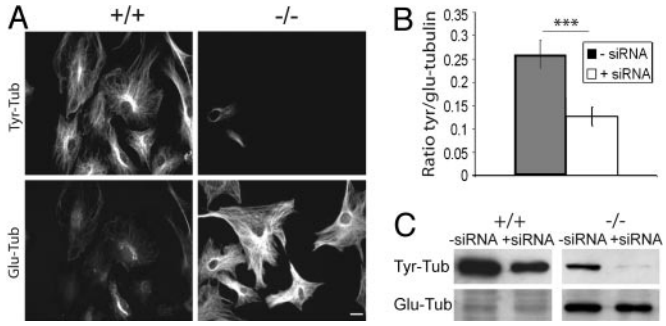

Fig. 2. Tyr-tubulin origin in TTL null fibroblasts. (*A*) Double-immunostaining of Tyr- and Glu-tubulin in WT (+/+) and TTL null (−/−) mouse embryonic fibroblasts treated with α-tubulin siRNA (see Fig. 8 for higher magnification). (Scale bar: 20 μm.) (*B*) Quantitative analysis of Tyr-/Glu-tubulin fluorescence intensity ratio in TTL null mouse embryonic fibroblasts. TTL null cells treated with α-tubulin siRNA ($n = 76$) showed a significant reduction in Tyr-/Glu-tubulin ratio compared with cells not treated with siRNA ($n = 66$). ***, $P < 0.001$ (*t* test). (*C*) Western blot analysis of Tyr- and Glu-tubulin in lysates of WT and TTL null mouse embryonic fibroblasts treated with Oligofectamine alone (−siRNA) or α-tubulin siRNA (+siRNA). Equal amounts of total protein were loaded.

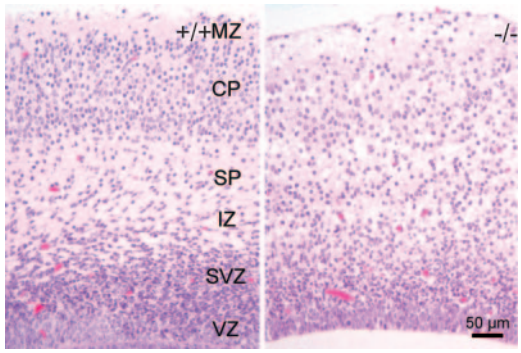

Fig. 3. Cortex anatomy. Coronal brain sections from WT (+/+) or TTL null (−/−) embryos (E19.5) were stained with hematoxylin and eosin. Note blurring of cortical layers in brains from TTL null mice with reduced cell numbers in the cortical plate zone (CP). MZ, mantle zone; SP, subplate zone; IZ, intermediate zone; SVZ, subventricular zone; VZ, ventricular zone.

However, TTL null mice displayed defective breathing and ataxia (data not shown) and died within 24 h after birth. TTL was undetectable in E19 TTL null tissues (Fig. 1*C*), and such tissue extracts revealed no TTL activity (data not shown), indicating full disruption of TTL expression.

Tubulin Composition in TTL Null Mice. α-Tubulin composition was probed in various tissues of WT and TTL null mice at E19 by using Tyr-, Glu-, and Δ2-tublin antibodies (10). Because of TTL suppression (12), Δ2-tublin was anomalously detectable in non-neuronal TTL null tissues (Fig. 1*D*). Because tubulin detyrosination occurs in differentiated cells (25), Glu-tubulin was detected in WT tissues. Surprisingly, minor amounts of Tyr-tubulin were present in TTL null tissues, especially in muscle; the reason is currently unknown. To examine Tyr-tubulin distribution and the consequences of TTL suppression in different cell types we analyzed cells derived from both WT and TTL null brain tissue by immunfluorescence (Fig. 1*E*). Oligodendrocytes (data not shown) as well as neurons and astrocytes of WT origin contained Tyr-tubulin, whereas both TTL null oligodendrocytes (data not shown) and neurons lacked detectable Tyr-tubulin (Fig. 1*E*; see also Fig. 7, which is published as supporting information on the PNAS web site). Examination of other cell types, including dividing fibroblasts (Fig. 2 and data not shown), also indicated that the residual Tyr-tubulin pool in TTL null tissues was unevenly distributed among cell types, being present mainly in dividing TTL null cells, but obviously not in postmitotic cells. Thus, an important question concerned the origin of Tyr-tubulin in such dividing TTL null cells.

Tyr-Tubulin Origin in TTL Null Cells. Tyr-tubulin in dividing TTL null cells could originate either from tubulin synthesis or a hitherto uncharacterized TTL enzymatic activity. Because the majority of fibroblasts derived from TTL null embryos revealed detectable amounts of Tyr-tubulin (see Fig. 8, which is published as supporting information on the PNAS web site), WT or TTL null fibroblasts were exposed to α-tubulin siRNA to suppress α-tubulin synthesis. After 48-h exposure the cell density was diminished and microtubule arrays were slightly disorganized but still almost exclusively composed of Tyr-tubulin in WT cells, whereas the number of Tyr-tubulin positive cells was drastically reduced in TTL null cultures (Figs. 2*A* and 8). A quantitative analysis of the Tyr/Glu-tubulin ratio (Fig. 2*B*) and Western blotting (Fig. 2*C*) showed a significant decrease of Tyr-tubulin after exposure of TTL null cells to α-tubulin siRNA. Two independent sets of siRNA gave similar results and demonstrated that, in dividing TTL null cells, Tyr-tubulin originates from tubulin synthesis.

Brain Anatomy in TTL Null Mice. No obvious malformation of any organ was detectable in newborn TTL null mice, and histological examination of a series of tissues, including lung, heart, liver, kidney, gut, trachea, and skin appeared normal (data not shown). Based on the symptoms of the newborn TTL null mice, we concentrated on the brain. At various stages of development, the general anatomic organization of the brain was conserved in TTL null mice, although variable extents of ventricular expansions were observed (data not shown). To investigate brain organization at the histological level, we focused on the cortex with its characteristic layer organization. Embryonic cerebral cortices at E13.5 showed an apparently normal preplate organization as indicated by calretinin staining (data not shown). At E19.5, the organization of the neocortex in cortical layers was clearly visible in WT embryos, whereas TTL null embryos displayed a blurred layer organization (Fig. 3). Appropriate formation of the cortex at late stages of development depends to a large extent on the establishment of correct reciprocal connections between the thalamus and the neocortex, forming the cortico-thalamic loop. In this context, previous work indicated that impairments of the cortico-thalamic loop development are lethal (26). This finding led us to analyze the establishment of the cortico-thalamic loop in TTL null mice.

Disruption of the Cortico-Thalamic Loop in TTL Null Brains. In the adult brain, the cortico-thalamic loop is characterized by axonal projections from the thalamus to the neocortex as well as from the neocortex to the thalamus (i.e., thalamocortical and cortico-thalamic pathways). In developing brains, the axons from the thalamus and the neocortex grow concurrently to eventually meet and form the internal capsule (IC). We used the lipophilic dye diI to label axonal projections in fixed E15 and E17 WT or TTL null brains (Fig. 4). Starting with thalamo-cortical projections at E15, diI implants in the thalamus labeled a thick bundle of axons forming the IC in WT specimen, which reached the intermediate zone of the ventral cortex as reported (27, 28) (Fig. 4*A*). In contrast, in TTL null brains, only a small fraction of labeled thalamic axons crossed the diencephalic-telencephalic boundary (DTB), but never formed the IC (Fig. 4*B*). By E17, numerous thalamic axons in WT brains had grown through the IC and extended toward the intermediate zone of the dorsal

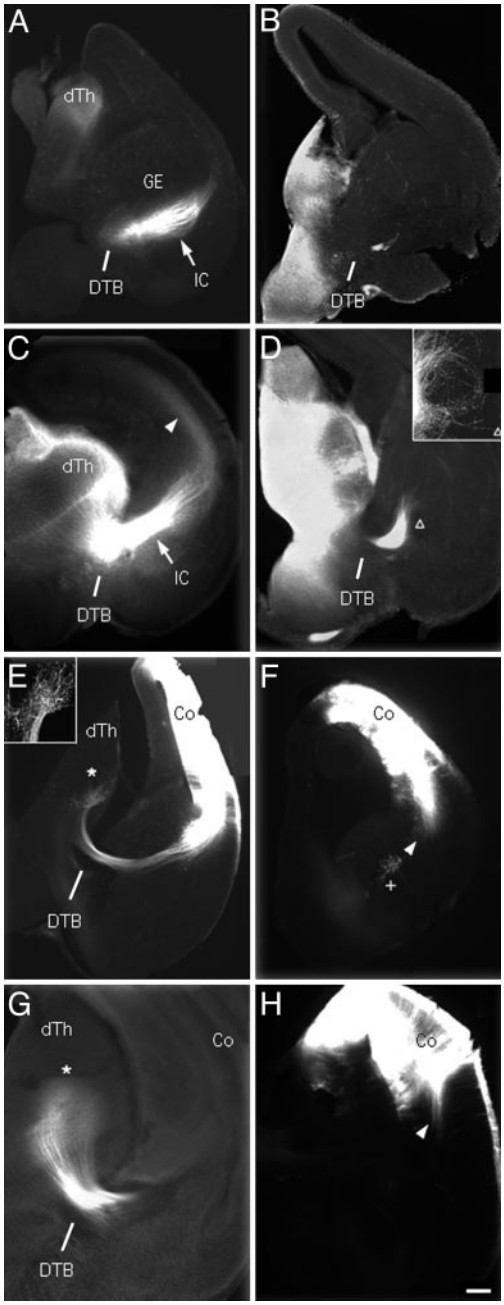

Fig. 4. Defective cortico-thalamic loop in embryonic TTL null mice. DiI labeling of the cortico-thalamic loop at E15 (*A*, *B*, *E*, and *F*) and E17 (*C*, *D*, *G*, and *H*) in WT (*Left*) or TTL null (*Right*) embryos, axon labeling after dil implants in the thalamus (*A–D*) or the cortex (*E–H*). (*A*) In E15 WT embryos, labeled thalamo-cortical axons grew through the IC (white arrow) up to the intermediate zone of the ventral cortex. (*B*) In contrast, in E15 TTL null embryos, a small bundle of labeled fibers just crossed the DTB, but did not form an IC. (*C*) In E17 WT embryos thalamo-cortical axons formed a thick bundle in IC (white arrow), and leading fibers reached their maximum extent in the intermediate zone of the dorsal cortex (white arrowhead). (*D*) In E17 TTL null embryos dil-labeled axons failed to form an IC, but wandered about in a looping trajectory (triangle and *Inset*). (*E*) Cortico-thalamic axons in E15 WT embryos formed a dense terminal projection zone in the thalamus (white star and *Inset*). (*F*) In E15 TTL null embryos, the maximum extent of labeled axons was restricted to the neocortex (white arrowhead). (*G*) In E17 WT embryos, labeled cortico-thalamic axons elaborate a dense terminal field (white star) whereas (*H*) in TTL null embryos the maximum extent reached by labeled axons is still confined to the neocortex as shown at E15 (compare white arrowheads in *F* and *H*). Co, cortex; dTh, dorsal thalamus. (Scale bar: 150 μm, *A–F*; 60 μm, *Insets* in *D* and *E*; and 75 μm, *G* and *H*.)

cortex (Fig. 4*C*). At the same age, labeled thalamic axons in TTL null brains did not form an appropriate IC but deviated from their normal route and looped around without further progress (Fig. 4*D*). We then examined cortico-thalamic projections from E15 to E17. In WT mice, the majority of labeled axons grew through the IC with the leading front reaching the thalamus (29) (Fig. 4*E*). In contrast, in TTL null brains, diI-labeled axons never exited the neocortex (Fig. 4*F*). In E17 WT brains, the vast majority of labeled cortico-thalamic axons projected densely to the thalamus and elaborated terminal arbors (Fig. 4*G*), whereas in TTL null mice, labeled axons were still restricted to the neocortex as shown at E15 (Fig. 4*H*). Thus, a major impairment of the cortico-thalamic loop in TTL null mice is obviously caused by abnormal neuronal projections *in vivo*.

Neuronal Differentiation of TTL Null Cells. We next tested whether the abnormal neuronal extensions observed in brain development were associated with impaired neurite outgrowth in isolated neurons. Neurons in primary culture follow a predictable temporal sequence of morphological changes as shown for hippocampal neurons (22) involving initial extension of a lamellipodial veil (stage I) that is later replaced by three to four minor neurites (stage II), one of which becomes the axon (stage III). This morphogenetic sequence is sensitive to cytoskeletal alterations (30, 31). Neuronal cells from E18.5 embryos, either WT or TTL null, were isolated, plated, and monitored for neurite extension and axon formation 12, 24, or 48 h later (Fig. 5*A*) in both cortical and hippocampal cultures. Whereas TTL null neurons reached each of the normal morphogenetic stages, axonal differentiation was premature, with a large excess of stage III cells (Fig. 5*A*; see also Fig. 9, which is published as supporting information on the PNAS web site). At day 2, when compared with WT cells all neurites and axons were longer in TTL null cells with an excess of abnormal cells with two axon-like extensions (tau-positive processes). Neurite growth pattern was further analyzed in stage II hippocampal neurons by video microscopy. Whereas neurites extended and retracted for short distances in WT cells, neurite growth was erratic in TTL null neurons, with growing and shrinking phases of large amplitude (Fig. 5*B*). A similar trend was observed in axons. Upon quantification, the neuritic growth rate, neuritic length variations, and axonal growth rate were significantly higher in TTL null cells (Fig. 5*B*). Thus, there were apparent defects in the control of neuritic growth in TTL null cells, with an erratic time course of neurite growth, an increased net rate of both neurite and axon extension, and apparent premature and abnormal axonal differentiation.

Abnormal CLIP170 Distribution in TTL Null Neurons. We did not detect any obvious disorganization of microtubule networks or actin organization in TTL null neurons. In particular, growth cones apparently had normal actin and microtubule organization (see Fig. 9), and we failed to find any perturbation in the expression or localization of major microtubule-associated proteins (MAPs) such as MAP2, MAP1B, STOPs, or of a variety of other microtubule proteins potentially involved in microtubule-dependent regulations of neurite outgrowth such as dynein, p150glued, or p140mDia (data not shown). The microtubule tip proteins EB1 and CLIP170 were of special interest because of their contribution to cell morphogenesis (31–37). Moreover, previous work in yeast suggested that tubulin detyrosination affects CLIP170 association with microtubule tips (38). In WT or TTL null developing neurons endogenous EB1 was distributed over the cell body and neurites, including growth cones, with distinct aspects of microtubule end labeling along the axon and in the growth cones (Fig. 6*A*; see also Fig. 10, which is published as supporting information on the PNAS web site). In WT neurons, CLIP170 had a similar general cellular distribution as EB1, although microtubule end labeling is not that distinct

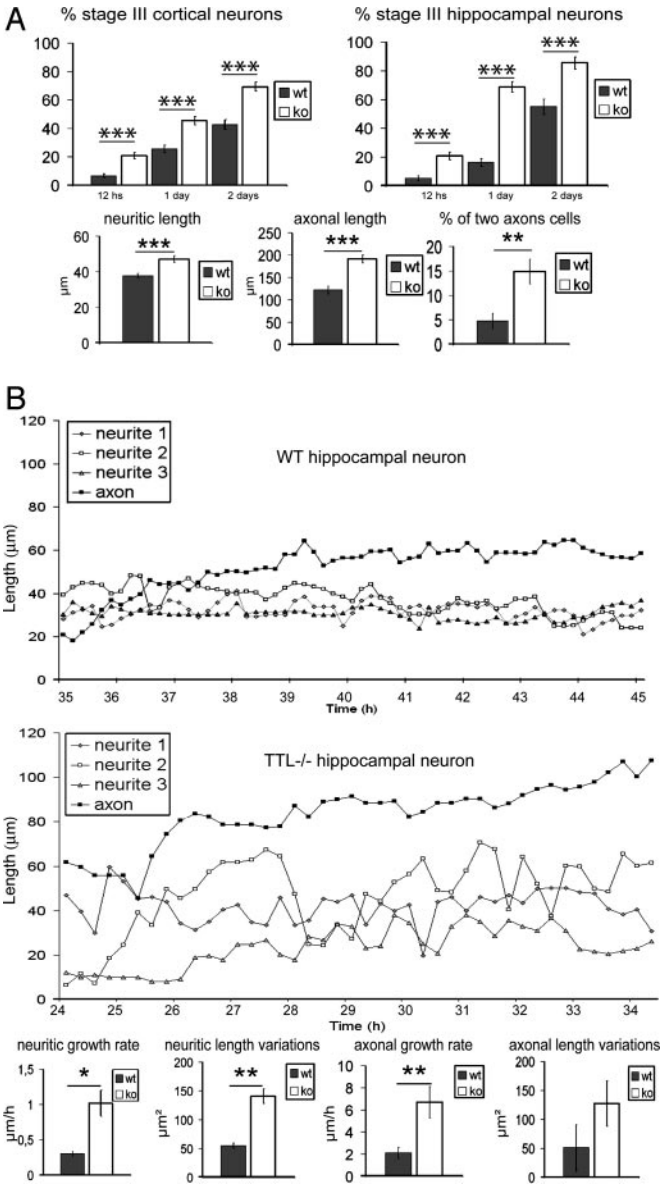

Fig. 5. Neurite outgrowth and axonal differentiation in cultured neurons. (*A*) Cell differentiation of cortical and hippocampal neurons in WT or TTL null primary culture after 0.5, 1, and 2 days *in vitro*. The percentage of cells reaching stage III (presence of an axon) was always increased in TTL null cells compared with WT cells, indicating a premature differentiation of TTL null neurons. Compared with WT cells in 2-day *in vitro* hippocampal cells, both neurite (WT, $n = 150$; TTL null, $n = 110$) and axonal (WT, $n = 50$; TTL null, $n = 75$) mean length were longer in TTL null cells. TTL null cultures also revealed a higher percentage of cells with two axon-like processes ($n = 190$ for both WT and TTL null). (*B*) Morphological changes during establishment of polarity in cultured hippocampal neurons examined by time-lapse, phase-contrast video microscopy. Neurite and axon growth was examined from 1 day after plating until 3 days, showing a 10-h sequence window including the phase of axon formation. Because axon differentiation is premature in TTL null cells, this window corresponds to different time points in WT and TTL null cultures. Quantification was performed by using the complete data. In WT hippocampal neurons, neurites extended and retracted over short distances over time. In TTL null neurons, neurites extended or retracted over markedly longer distances. The net rate of neurite (WT, $n = 16$; TTL null, $n = 18$) and axonal (WT, $n = 9$; TTL null, $n = 10$) elongation was increased in TTL null cells compared with WT cells. Neuritic length variations (measured as the linked variance of neuritic length around the linear regression of length vs. time) were significantly higher in TTL null neurons compared with WT neurons.

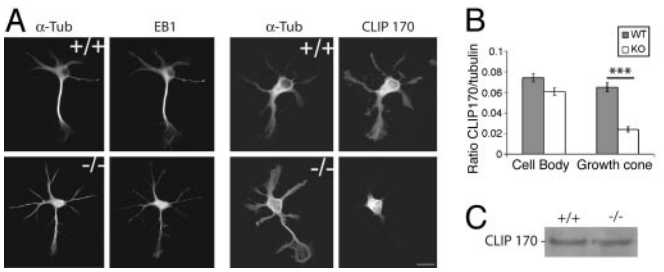

Fig. 6. Distribution of EB1 and CLIP170 in hippocampal neurons. (*A*) Double-immunofluorescence of EB1/α-tubulin and CLIP170/α-tubulin in WT and TTL null neurons. In both, EB1 is distributed throughout the cell body, neurites, and growth cones with a characteristic ''comet'' pattern. In WT neurons, CLIP170 is also distributed throughout the cell body, neurites, and growth cones, whereas in TTL null neurons, the CLIP170 signal is restricted to the cell body and initial parts of neurites, being undetectable in growth cones (see Fig. 10 for higher magnification). (Scale bar: 10 μm.) (*B*) Quantitative analysis of CLIP 170 staining, showing CLIP170/α-tubulin fluorescence intensity ratios in cell bodies (WT, $n = 32$; TTL null, $n = 41$) or growth cones from WT or TTL null neurons (WT, $n = 30$; TTL null, $n = 27$). Growth cones of TTL null neurons showed a significant reduction in CLIP170 levels compared with WT cells. ***, $P < 0.001$ (*t* test). (*C*) Immunoblot analysis of CLIP170 content in WT or TTL null neurons. Equal amounts of total protein were loaded.

with CLIP170 antibodies, whereas in TTL null neurons, CLIP170 was detectable in the cell body in similar amounts as in WT neurons, but was drastically diminished in neurite extensions and growth cones (Figs. 6*B* and 10) despite similar expression levels (Fig. 6*C*). Thus, CLIP170 was mislocalized in TTL null neurons.

Discussion

In this study we inactivated a key enzyme involved in a tubulin modification in whole mammals, with dramatic consequences on brain development and animal survival. TTL suppression led to abnormal expression of Δ2-tublin in nonneuronal tissues, with no obvious effects on organ development, suggesting that Δ2-tubulin accumulation *per se* is not deleterious to cells. Whereas TTL suppression fully depleted Tyr-tubulin in postmitotic cells, such as neurons, Tyr-tubulin persisted in dividing TTL null cells where it apparently arose from tubulin synthesis, which probably is more active in dividing cells than in quiescent cells to provide sufficient amounts of tubulin to daughter cells. Currently we do not know whether the rescue pool of newly synthesized Tyr-tubulin is essential for the progression of the cell cycle in dividing TTL null cells. TTL activity is highest in the brain (2), and Tyr-tubulin suppression in TTL null neurons apparently caused extensive disorders in neuronal organization, including a disruption of the cortico-thalamic loop. Further detailed analysis of TTL null brain organization strongly suggests that anomalies in neuronal growth affect other neurons in addition to cortico-thalamic neurons (E. Bloch-Gallego, personal communication). However, the disruption of the cortico-thalamic loop is probably sufficient to account for the perinatal death of TTL null newborns, as other mouse mutants such as Mash-1- or Pax-6-deficient mice with disrupted cortico-thalamic loops are not viable (26). Disruption of the cortico-thalamic loop in TTL null mice could have various origins such as anomalies in neurite extension formation. Whereas cortical neurite projections are shorter in the brain of TTL null mice, neurites grow faster and differentiate earlier in cultured TTL null neurons than in WT neurons. TTL null cells also show an erratic time course of neurite outgrowth and anomalies of axonal differentiation. Apparently, TTL suppression disrupted mechanisms that are essential for controlling neurite outgrowth, but not neurite outgrowth *per se*. Disruption of the cortico-thalamic loop could

CELL BIOLOGY

result, at least in part, from the lack of a "handshake" between thalamo-cortical and cortico-thalamic projections (39), which crucially depends on a correct time and space control of axonal growth.

Based on recent evidence in *Saccharomyces cerevisiae*, indicating a specific and crucial role of the C-terminal aromatic residue of α-tubulin for CLIP170 association with microtubule tips (38), we analyzed CLIP170 localization in WT and TTL null neurons, which could be important for the control of cell morphogenesis (40) and the dynamic control of adhesive structures (41). CLIP170 is mislocalized in TTL null neurons, being absent from neurite extensions and growth cones, which may contribute to impaired control of neurite extensions in TTL null neurons. Further studies are required to decipher the downstream consequences of CLIP170 mislocalization that may reveal additional anomalies. For instance, although TTL suppression does not affect microtubule dynamics by itself (12), we have observed increased microtubule resistance to nocodazole in developing TTL null neurons (data not shown), which may be a consequence of CLIP170 mislocalization and whose importance for the TTL null phenotype needs to be assessed. In any case, detailed studies of CLIP170 interactions with microtubules, the composition of microtubule tip complexes, and microtubule dynamics are required.

We thank D. Proietto for technical assistance, Dr. E. Bloch-Gallego for communication of unpublished data, Dr. F. Perez for help and advice, and several colleagues for discussion. This work was supported by la Ligue Nationale Contre le Cancer (Équipe Labellisée Ligue) (D.J.), Association de la Recerche sur le Cancer Grant 9041 (to M.V.), and the Deutsche Forschungsgemeinschaft and the Fonds der Chemischen Industrie (J.W.).

1. Westermann, S. & Weber, K. (2003) *Nat. Rev. Mol. Cell Biol.* **4,** 938–947.
2. Barra, H. S., Arce, C. A. & Argarana, C. E. (1988) *Mol. Neurobiol.* **2,** 133–153.
3. Ersfeld, K., Wehland, J., Plessmann, U., Dodemont, H., Gerke, V. & Weber, K. (1993) *J. Cell Biol.* **120,** 725–732.
4. Barra, H. S., Rodriguez, J. A., Arce, C. A. & Caputto, R. (1973) *J. Neurochem.* **20,** 97–108.
5. Preston, S. F., Deanin, G. G., Hanson, R. K. & Gordon, M. W. (1979) *J. Mol. Evol.* **13,** 233–244.
6. Gundersen, G. G., Kalnoski, M. H. & Bulinski, J. C. (1984) *Cell* **38,** 779–789.
7. Kreis, T. E. (1987) *EMBO J.* **6,** 2597–2606.
8. Wehland, J. & Weber, K. (1987) *J. Cell Sci.* **88,** 185–203.
9. Paturle-Lafanechere, L., Edde, B., Denoulet, P., Van Dorsselaer, A., Mazarguil, H., Le Caer, J. P., Wehland, J. & Job, D. (1991) *Biochemistry* **30,** 10523–10528.
10. Paturle-Lafanechere, L., Manier, M., Trigault, N., Pirollet, F., Mazarguil, H. & Job, D. (1994) *J. Cell Sci.* **107,** 1529–1543.
11. Webster, D. R., Wehland, J., Weber, K. & Borisy, G. G. (1990) *J. Cell Biol.* **111,** 113–122.
12. Lafanechere, L., Courtay-Cahen, C., Kawakami, T., Jacrot, M., Rudiger, M., Wehland, J., Job, D. & Margolis, R. L. (1998) *J. Cell Sci.* **111,** 171–181.
13. Mialhe, A., Lafanechere, L., Treilleux, I., Peloux, N., Dumontet, C., Bremond, A., Panh, M. H., Payan, R., Wehland, J., Margolis, R. L. & Job, D. (2001) *Cancer Res.* **61,** 5024–5027.
14. Kato, C., Miyazaki, K., Nakagawa, A., Ohira, M., Nakamura, Y., Ozaki, T., Imai, T. & Nakagawara, A. (2004) *Int. J. Cancer* **112,** 365–375.
15. Erck, C., MacLeod, R. A. & Wehland, J. (2003) *Cytogenet. Genome Res.* **101,** 47–53.
16. Tybulewicz, V. L., Crawford, C. E., Jackson, P. K., Bronson, R. T. & Mulligan, R. C. (1991) *Cell* **65,** 1153–1163.
17. Nagy, A., Rossant, J., Nagy, R., Abramow-Newerly, W. & Roder, J. C. (1993) *Proc. Natl. Acad. Sci. USA* **90,** 8424–8428.
18. Pirollet, F., Margolis, R. L. & Job, D. (1992) *Biochim. Biophys. Acta* **1160,** 113–119.
19. Rickard, J. E. & Kreis, T. E. (1991) *J. Biol. Chem.* **266,** 15597–15605.
20. Wehland, J. & Weber, K. (1987) *J. Cell Biol.* **104,** 1059–1067.
21. Godement, P., Vanselow, J., Thanos, S. & Bonhoeffer, F. (1987) *Development (Cambridge, U.K.)* **101,** 697–713.
22. Dotti, C. G., Sullivan, C. A. & Banker, G. A. (1988) *J. Neurosci.* **8,** 1454–1468.
23. Ainger, K., Avossa, D., Morgan, F., Hill, S. J., Barry, C., Barbarese, E. & Carson, J. H. (1993) *J. Cell Biol.* **123,** 431–441.
24. Elbashir, S. M., Harborth, J., Weber, K. & Tuschl, T. (2002) *Methods* **26,** 199–213.
25. Gundersen, G. G. & Bulinski, J. C. (1986) *Eur. J. Cell Biol.* **42,** 288–294.
26. Lopez-Bendito, G. & Molnar, Z. (2003) *Nat. Rev. Neurosci.* **4,** 276–289.
27. Molnar, Z., Adams, R. & Blakemore, C. (1998) *J. Neurosci.* **18,** 5723–5745.
28. Braisted, J. E., Catalano, S. M., Stimac, R., Kennedy, T. E., Tessier-Lavigne, M., Shatz, C. J. & O'Leary, D. D. (2000) *J. Neurosci.* **20,** 5792–5801.
29. Hevner, R. F., Miyashita-Lin, E. & Rubenstein, J. L. (2002) *J. Comp. Neurol.* **447,** 8–17.
30. da Silva, J. S. & Dotti, C. G. (2002) *Nat. Rev. Neurosci.* **3,** 694–704.
31. Dehmelt, L. & Halpain, S. (2004) *J. Neurobiol.* **58,** 18–33.
32. Beach, D. L., Thibodeaux, J., Maddox, P., Yeh, E. & Bloom, K. (2000) *Curr. Biol.* **10,** 1497–1506.
33. Brunner, D. & Nurse, P. (2000) *Cell* **102,** 695–704.
34. Busson, S., Dujardin, D., Moreau, A., Dompierre, J. & De Mey, J. R. (1998) *Curr. Biol.* **8,** 541–544.
35. Carvalho, P., Tirnauer, J. S. & Pellman, D. (2003) *Trends Cell Biol.* **13,** 229–237.
36. Coquelle, F. M., Caspi, M., Cordelieres, F. P., Dompierre, J. P., Dujardin, D. L., Koifman, C., Martin, P., Hoogenraad, C. C., Akhmanova, A., Galjart, N., *et al.* (2002) *Mol. Cell. Biol.* **22,** 3089–3102.
37. Maddox, P. S., Stemple, J. K., Satterwhite, L., Salmon, E. D. & Bloom, K. (2003) *Curr. Biol.* **13,** 1423–1428.
38. Badin-Larcon, A. C., Boscheron, C., Soleilhac, J. M., Piel, M., Mann, C., Denarier, E., Fourest-Lieuvin, A., Lafanechere, L., Bornens, M. & Job, D. (2004) *Proc. Natl. Acad. Sci. USA* **101,** 5577–5582.
39. Molnar, Z. & Blakemore, C. (1995) *Trends Neurosci.* **18,** 389–397.
40. Busch, K. E., Hayles, J., Nurse, P. & Brunner, D. (2004) *Dev. Cell* **6,** 831–843.
41. Krylyshkina, O., Anderson, K. I., Kaverina, I., Upmann, I., Manstein, D. J., Small, J. V. & Toomre, D. K. (2003) *J. Cell Biol.* **161,** 853–859.